Regular Article – Experimental Physics

Charmed particles production in pA-interactions at $\sqrt{s} = 11.8$ GeV

SVD-2 Collaboration

A. Aleev[1], E. Ardashev[2], A. Afonin[2], V. Balandin[1], S. Basiladze[3], G. Bogdanova[3], M. Bogolyubsky[2], M. Boguslavsky[1], V. Dunun[1], O. Gavrishchuk[1], S. Golovnia[2], S. Gorokhov[2], V. Golovkin[2], N. Grishin[3], Ya. Grishkevich[3], P. Ermolov[3], N. Furmanec[1], D. Karmanov[3], A. Kholodenko[2], V. Kireev[1], A. Kiriyakov[2], V. Konstantinov[1], I. Kosarev[1], E. Kokoulina[1,a], V. Kozlov[3], V. Kramarenko[3], A. Kubarovsky[3], N. Kuzmin[1], L. Kurchaninov[2], G. Lanshikov[1], A. Larichev[3], A. Leflat[3], S. Lyutov[3], M. Merkin[3], G. Mitrofanov[2], A. Moiseev[2], V. Nikitin[1], S. Orfanitsky[3], V. Petrov[2], Yu. Petukhov[1], A. Pleskach[2], V. Popov[3], V. Riadovikov[2], V. Ronjin[2], I. Rufanov[1], V. Senko[2], N. Shalanda[2], M. Soldatov[2], L. Tikhonova[3], T. Topuria[1], Yu. Tsyupa[2], M. Vasiliev[2], A. Vischnevskaya[3], V. Volkov[3], A. Vorobiev[2], A. Voronin[3], V. Yakimchuk[2], A. Yukaev[1], V. Zapolsky[2], V. Zmushko[2], S. Zotkin[3], D. Zotkin[3], and E. Zverev[3]

[1] Joint Institute for Nuclear Research, St. Joliot-Curie 6, Dubna, Moscow region, 141980, Russia
[2] Institute for High Energy Physics, Sq. Nauki 1, Protvino, Moscow region, 142281, Russia
[3] Federal State Budget Educational Institution of Higher Education M.V. Lomonosov, Moscow State University, Skobeltsyn Institute of Nuclear Physics (SINP MSU), 1(2), Leninskie gory, GSP-1, Moscow 119991, Russia

Abstract. The results of the SERP-E-184 experiment at the U-70 accelerator (IHEP, Protvino) are presented. Interactions of the 70 GeV proton beam with carbon, silicon and lead targets were studied to detect decays of charmed D^0, $\bar{D}^0$, D^+, D^- mesons and Λ_c^+ baryon near their production threshold. Measurements of lifetimes and masses have shown a good agreement with PDG data. The inclusive cross-sections of charm production and their A-dependences have been obtained. The yields of these particles are compared with the theoretical predictions and the data of other experiments. The measured cross-section of the total open charm production ($\sigma_{\rm tot}(c\bar{c}) = 7.1 \pm 2.3(\text{stat}) \pm 1.4(\text{syst})\,\mu\text{b/nucleon}$) at the collision c.m. energy $\sqrt{s} = 11.8$ GeV is well above the QCD model predictions. The contributions of different kinds of charmed particles to the total cross-section of the open charm production in proton-nucleus interactions vary with energy.

1 Introduction

The last decades have seen an intensive development of charm physics. The increased energy of accelerators allowed one to investigate rare events, search for new physics beyond the standard model and the discovery of new states of the nuclear matter. Most of the experiments on charm have been carried out with electron beams (measurements of mass, branching ratios etc.). Experiments with hadron and heavy ion beams gave an opportunity to study mechanisms of charmed particle production in varying nuclear media from low energy ($\sqrt{s} < 30$ GeV) up to the LHC energy (TeV region). It has been found that charmed hadron production is sensitive to medium modifications. And vice versa, charmed particles are good probes to investigate properties of this medium. For a bet-

ter understanding of the strong interaction mechanisms, in particular of the hadronization of heavy quarks, one should investigate the low energy domain near the threshold of charmed hadron production. The investigations of the low energy region are proposed in the CBM experiment at the future FAIR facility [1]. This experiment will measure heavy ion interactions as well, but the maximum energy accessible by CBM will be well below the energy of the SERP-E-184 experiment.

The measurements of the cross-sections of the charmed particle production at the near-threshold energy region were performed more than 20 years ago at the Institute for High Energy Physics (IHEP, Protvino) by the beam-dump experiment with a muon absorber [2], by the SCAT bubble chamber experiment [3] and by the experiment with the BIS-2 spectrometer [4]. The measured total cross-sections in the energy range of the primary beam from 40 to 70 GeV have proved to be much higher than the model
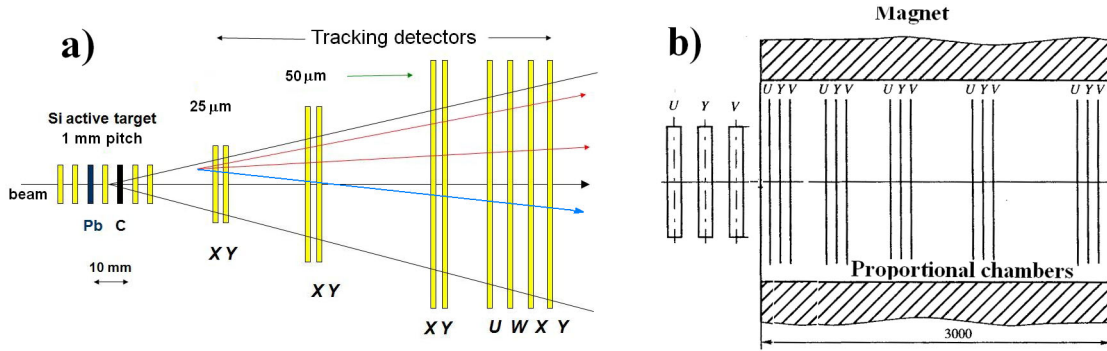

Fig. 1. a) The micro-strip vertex detector (MSVD) and b) the magnetic spectrometer (MS).

predictions based on QCD. On the other hand, in the experiments at the energy of incident protons higher than 200 GeV the total cross-section is in agreement with the QCD-based models [5].

The SERP-E-184 experiment at the U-70 accelerator (IHEP, Protvino) was carried out at the SVD-2 (Spectrometer with Vertex Detector, second version) setup. This setup was constructed to study the charmed particle production in pp- and pA-interactions by the SVD Collaboration. A detailed description of the SVD setup can be found in [6].

In sect. 2, the main characteristics of the SVD-2 setup are presented. In sect. 3 we describe the simulations of charmed particle production, their registration with our setup and software. The selection of events with charmed particles is shown in sect. 4. The summarized results are presented in sect. 5. Section 6 gives the conclusions.

2 SVD setup detectors

The main elements of the setup for charm searching are the high-precision micro-strip vertex detector (MSVD) with an active target (AT) and a magnetic spectrometer (MS).

The active target (AT) (fig. 1) contains 5 Si-detectors each $300\,\mu$m thick and 1 mm pitch strips, a Pb-plate ($220\,\mu$m thick) and a C-plate ($500\,\mu$m thick), placed as Si-Si-Pb-Si-C-Si-Si. All inter-plane distances were set to 4 mm. The total thickness of the target was 0.5% of interaction lengths. The micro-strip tracking part of MSVD consists of 10 Si-detectors: a XY pair which has 640 strips with a $25\,\mu$m pitch; a XY pair —640 strips with a $50\,\mu$m pitch; a XY pair —1024 strips having a $50\,\mu$m pitch and a $XYUV$ quadruplet —1024 strips and a $50\,\mu$m pitch. U and V are oblique planes. The angular acceptance of MSVD was ±250 mrad.

The large aperture magnetic spectrometer (MS) consists of the electromagnet with an aperture of $1.8 \times 1.2\,\mathrm{m^2}$ and homogenous field of 1.18 T over a 3 m long region. Two sets of multiwire proportional chambers are placed before and inside the magnet. The first one has 1 UYV triplet ($1.0 \times 1.0\,\mathrm{m^2}$), the second one has 5 UYV triplets ($1.0 \times 1.5\,\mathrm{m^2}$). The interwire distances are 2 mm for each of the chambers. The total number of planes is 18, and the total number of signal wires is ~ 18000. The angu-
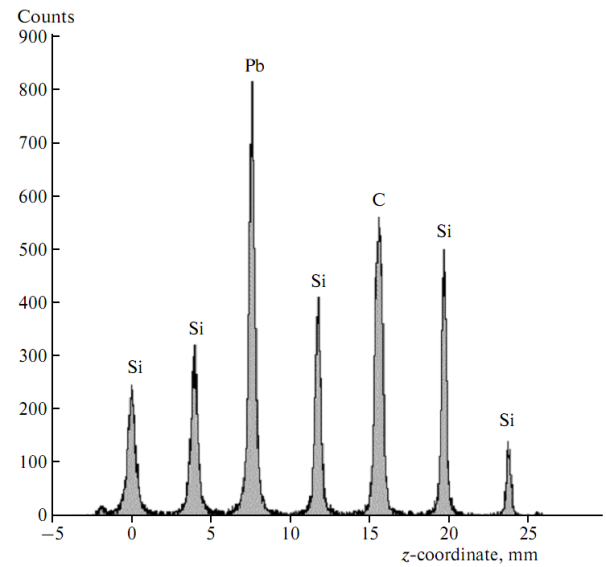

Fig. 2. The reconstructed Z-coordinates of the primary vertices in AT.

lar acceptance of the spectrometer is ±200 mrad for the horizontal coordinate and ±150 mrad for the vertical one.

The trigger system selected the minimum bias events using signals from the scintillation counters, placed before the AT, and from the active target strips. A more detailed description of the trigger logic and the data acquisition system can be found elsewhere [6].

The primary vertex space resolutions were calculated as 70–120 μm for the Z-coordinate (fig. 2) along the beam particle depending on the multiplicity of the events and 8–12 μm for the X and Y coordinates in the perpendicular plane to it. For two-prong secondary vertices (K_s^0, Λ^0) these values were $250\,\mu$m and $15\,\mu$m, respectively. The impact parameter (the distance between track and primary vertex) for 3–5 GeV momentum tracks was measured with a precision of $12\,\mu$m.

The spectrometer features allow one to get an effective mass resolution of $\sigma = 4.4\,\mathrm{MeV}/c^2$ for K_s^0 and $1.6\,\mathrm{MeV}/c^2$ for Λ^0 masses, for the particles decayed before the MSVD tracking detectors. The momentum resolution for the tracks with 15 and more measured hits in MS planes was $(0.5$–$1.0)\%$ in the (4–20) GeV momentum range. The angular error was estimated as 0.2–0.3 mrad.

The pencil proton beam was extracted from the U-70 accelerator by the bent crystal deflector system. The beam transverse size on the target was ~ 2 mm. The data acquisition run was performed with the 70 GeV proton beam of intensity of $(5\text{–}6)\cdot 10^5$ p/s. In total, $5.2\cdot 10^7$ inelastic events were collected.

3 Simulations and data processing

Proton-nucleus interactions were simulated by means of the FRITIOF7.02 code [7]. It treats hadronic events as independent collisions of an incident particle with the nucleons of the target. The Fermi motion of nucleons, the deformation of the nucleus and multiple re-scattering are taken into account. The nucleon distribution density in a nucleus is described in our case by the Woods-Saxon potential $\rho(r) = \frac{\rho(0)}{1+\exp[(r-r(0)A^{1/3})/c]}$, with $r(0) = 1.16 \cdot (1 - 1.16A^{-2/3})$ fm and $c = 0.5$ fm. The production of quark-antiquark pairs in minimum bias events was simulated within the dipole cascade model, with hadronization processes described by the Lund scheme using the fragmentation function $f(z) \sim z^{-1}(1-z)^a \cdot \exp(-bm_t^2/z)$. The parameters of this function were chosen as $a = 0.18$ and $b = 0.34$ GeV^{-2} in accordance with the results of the e^+e^- experiments OPAL [8] and CLEO [9], where the parameters were adjusted by the measured spectra of D and D^* mesons. Default values were used for the remaining parameters in the FRITIOF code.

Monte Carlo (MC) events were obtained with FRITIOF separately for interactions on carbon, silicon, and lead with charm production. A good agreement with MC and experimental events after their reconstruction was found for the numbers of minimum bias events in each of the AT plates, for multiplicities of charged particles in primary vertices and for their momenta. Decays of unstable particles and particle tracking were performed within GEANT3.21 [10]. Certain decay modes were imposed for charmed particles ($D^0 \to K^-\pi^+$, $\bar{D}^0 \to K^+\pi^-$, $D^+ \to K^-\pi^+\pi^+$, $D^- \to K^+\pi^-\pi^-$, $\Lambda_c^+ \to pK^-\pi^+$).

The geometry of active and passive elements of the setup was defined by means of metrological measurements and corrected with the results of the "straight tracks" software alignment. The measured grid map of the magnetic field was applied. Charge spreading over the MSVD strips, noise and cutoff amplitudes were introduced channel-by-channel in accordance with experimentally measured values and data acquisition parameters. The actual efficiencies obtained experimentally for the proportional wire chambers were used for the magnetic spectrometer.

The real and Monte Carlo data were reconstructed by the data processing system of the SERP-E-184 experiment. The data processing procedure started with the filtration of MSVD data and reconstruction of tracks and primary vertices [11]. Next, we selected events with a secondary vertex close to the interaction point as candidates for charm production events. For this purpose, the method of the analysis in the space of track parameters [12] was applied. In this space each track is presented with a point
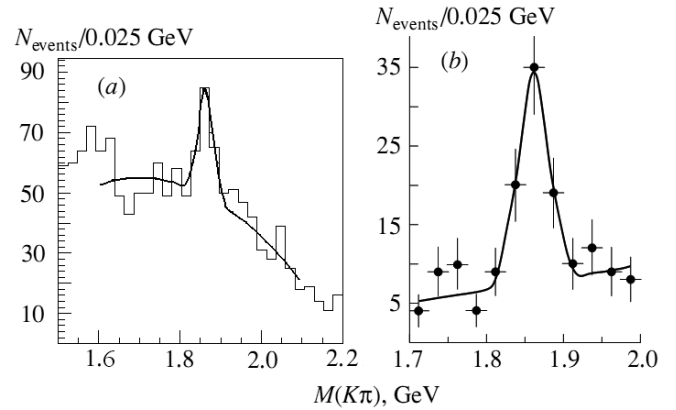

Fig. 3. Effective mass spectra of the $K\pi$ system (a) before and (b) after visual inspection.

and all points for the tracks from the same vertex are located on a straight line. The common part ended with the geometric reconstruction of the tracks in the MS to determine the momenta of charged particles. The event selection and analysis, including its kinematics, were specific for each goal: neutral or charged D mesons and Λ_c^+. The particle detection efficiency is calculated after this. Using the simulated charm production events we have elaborated and optimized criteria to select events with decays in the vicinity of the primary interaction vertex. The results of simulations were compared with the experimental data. The same selection criteria are applied for experimental and simulated events.

In case of the $D^0(\bar{D}^0) \to K\pi$ process, the detection of $K_s^0 \to \pi\pi$ decay in the MSVD can serve as a reference procedure, because the well-known kaon production cross-section is many times larger than for charmed particles. It was used to estimate the detection efficiency of the V^0 decay near the primary vertex and to validate the data processing algorithms for the $D^0(\bar{D}^0)$ meson [13].

Additionally, the background minimum bias events were simulated without charm production. This procedure was necessary to estimate background conditions. The characteristics of three-prong systems ($K\pi\pi$ and $pK\pi$) for MC events were compared to the experimental data [14, 15]. There is a good agreement between the simulated and experimental distributions for path length, momentum and x_F variable ($x_F = 2p_\parallel/\sqrt{s}$ in the c.m.s.).

4 Selection of events with charmed particles

4.1 $D^0 \to K^-\pi^+$, $\bar{D}^0 \to K^+\pi^-$

Candidates for events with D^0 or $\bar{D}^0$ particles and their decay into the $K\pi$ system were selected using the criteria presented in [13]. The effective mass spectra of the $K\pi$ system after applying these criteria and visual inspection of the events by the physicists are shown in figs. 3(a) and (b).

The mass interval for the visual inspection was limited to the region from 1.7 to 2.0 GeV/c^2. The visual inspection significantly reduces the background by 85% in the region

Table 1. The results of the effective mass spectra fitting and the parameter $c\tau$.

Particle decay	Signal events	Background events	χ^2/NDF	Detection efficiency	Mass, GeV/c^2 (*PDG mass*)	$c\tau$, mm (*PDG $c\tau$*)
$D^0 \to K\pi$	51 ± 17	38 ± 13	5.5/6	0.036	1861 ± 7 (*1864.8*)	$0.123 \pm 0.014 \pm 0.010$ (*0.124*)
$D^+ \to K^-\pi^+\pi^+$	15.5 ± 5.6	16.6 ± 6.0	13.5/30	0.014	1874 ± 5 (*1869.6*)	$0.291 \pm 0.075 \pm 0.078$ (*0.311*)
$D^- \to K^+\pi^-\pi^-$	15.0 ± 4.7	8.7 ± 2.7	3.6/20	0.008	1864 ± 8 (*1869.6*)	$0.341 \pm 0.088 \pm 0.068$ (*0.311*)
$\Lambda_c^+ \to pK^-\pi^+$	21.6 ± 6.0	16 ± 4	12.7/33	0.011	2287 ± 4 (*2286.5*)	$0.051 \pm 0.011 \pm 0.015$ (*0.059*)
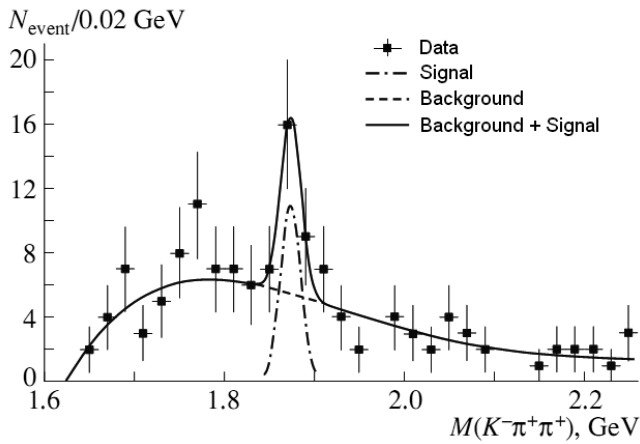
Fig. 4. Effective mass spectrum of the $K^-\pi^+\pi^+$ system after implementation of all selection criteria. The solid line shows the result of the fit by the sum of a Gaussian function and a fifth-order polynomial.
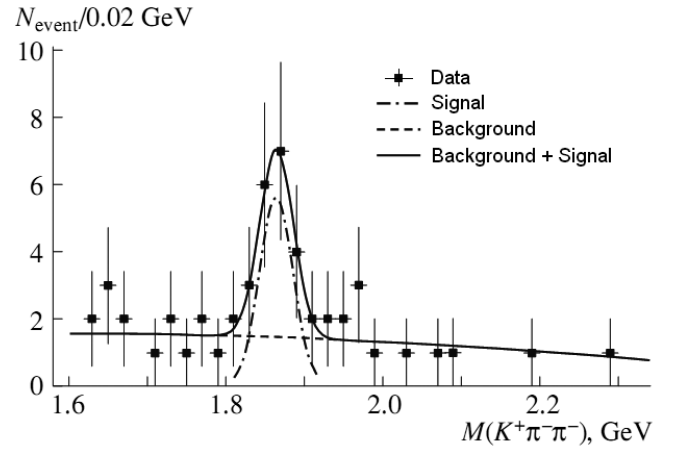
Fig. 5. The effective mass spectrum of the $K^+\pi^-\pi^-$ system after using all selection criteria. The solid line shows the fit by the sum of a Gaussian function and a second-order polynomial.

of interest, while the charm + anti-charm ($D^0 + \bar{D}^0$) signal decreased only by 30%.

The data fit by the sum of a straight line and a Gaussian function is shown in fig. 3(b). It gives $(1861 \pm 7)\,\text{MeV}/c^2$ in agreement with the world average value (see table 1) for the D^0 or $\bar{D}^0$ mass with a σ of $21\,\text{MeV}/c^2$ (χ^2/NDF = 5.5/6). We obtained 51 ± 17 signal events from the D^0 or $\bar{D}^0$ meson decay over a background of 38 ± 13 events. The detection efficiency of $D^0 + \bar{D}^0$ particles with the efficiency of the visual inspection technique is equal to $\varepsilon(D^0 + \bar{D}^0) = 0.036$.

The total acceptance (geometrical acceptance and detection efficiencies) of the SVD-2 setup makes it possible to measure the transverse momentum ($p_{\rm t}$) and the Feynman variable ($x_{\rm F}$) of neutral charmed mesons over a broad region spanned by $p_{\rm t}^2$ between 0 and 4 $(\text{GeV}/c)^2$ and $x_{\rm F}$ between -0.2 and $+0.6$.

4.2 $D^+ \to K^-\pi^+\pi^+$, $D^- \to K^+\pi^-\pi^-$

Charged charmed mesons were found by analyzing events with a three-prong secondary vertex. The selection procedure of events was presented in details in [14].

Figure 4 shows the effective mass spectrum of the $K^-\pi^+\pi^+$ system for the experimental events after all selection criteria were applied. After parameterizing the spectrum in fig. 4 in terms of the sum of a Gaussian function and a fifth-order polynomial (χ^2/NDF = 13.5/30), we obtained 15.5 ± 5.6 signal events from the D^+ meson decay over a background of 16.6 ± 6.0 events. The measured D^+ meson mass is $(1874 \pm 5)\,\text{MeV}/c^2$ in agreement with the world average value (see table 1) with a σ of $11\,\text{MeV}/c^2$. The detection efficiency $\varepsilon(D^+) = 0.014$ was determined from simulations.

The same procedure was applied to search for the D^- meson signal (fig. 5) in the mass spectrum of the $K^+\pi^-\pi^-$, which was parameterized as a sum of a Gaussian function and a second-order polynomial (χ^2/NDF = 3.6/20).

The number of events in the signal is 15.0 ± 4.7 over a background of 8.7 ± 2.7 events. The D^- meson mass was $(1864 \pm 8)\,\text{MeV}/c^2$ in agreement with the world average value (see table 1) with a σ of $22\,\text{MeV}/c^2$. The detection efficiency obtained through simulations for the D^- meson signal is equal to $\varepsilon(D^-) = 0.008$. The phase space coverage of both reconstructed charged D mesons is $0 < p_{\rm t}^2 < 4$ $(\text{GeV}/c)^2$ and $-0.1 < x_{\rm F} < +0.4$.
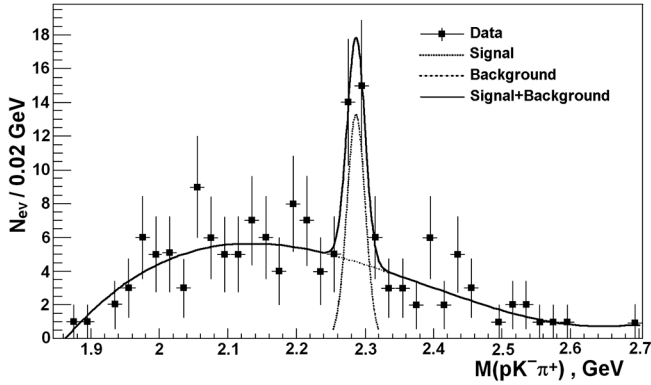
Fig. 6. The effective mass spectrum of the $pK^-\pi^+$ system after using all selection criteria. The solid line shows the fit by the sum of a Gaussian function and a third-order polynomial.

4.3 $\Lambda_c^+ \to pK^-\pi^+$

The selection procedure of the events was presented in detail in [15]. Without particle identification, we had two hypotheses for positively charged particles of the $(pK^-\pi^+)$ system in the effective mass spectrum.

The application of all criteria resulted in the effective mass spectrum shown in fig. 6, which was parameterized by the sum of a Gaussian function and a third-order polynomial ($\chi^2/\mathrm{NDF} = 12.7/33$). The fit returned a mass value of $(2287 \pm 4)\,\mathrm{MeV}/c^2$ in agreement with the world average value (see table 1) and a σ of $13.1\,\mathrm{MeV}/c^2$. We obtained a Λ_c^+ signal of 21.6 ± 6.0 events over a background of 16 ± 4 events. The detection efficiency for $\Lambda_c^+ \to pK^-\pi^+$ is equal to $\epsilon = 0.011$. For reconstructed Λ_c^+ baryons, the phase space coverage is $0 < p_t^2 < 2.5\,(\mathrm{GeV}/c)^2$ and $0 < x_\mathrm{F} < 0.8$. When both hypotheses turned out to be in the peak region, they are taken with weights of 0.5 (there were 5% of such events in simulations and none in the experimental data).

A summary of the fit results to the effective spectra discussed above and the measured parameter $c\tau$ are presented in table 1.

The decay lengths for charmed particles measured in this experiment (table 1) are in agreement within errors with the PDG data [16]. The estimates of $c\tau$ for regions off the signal region differ substantially from those values.

5 Cross-sections for charmed particle production and their A-dependence

The following relation was used to calculate the inclusive cross-sections for a given charmed particle:

$$N_\mathrm{s}(i) = [N_0 \times (\sigma(i) \times A^\alpha)/(\sigma_{pp} \times A^{0.7})] \times [(B(i) \times \varepsilon(i))/K_\mathrm{tr}],$$

where $i = D^0$, $\bar{D}^0$, D^+, D^- or Λ_c^+; $N_\mathrm{s}(i)$ is the number of signal events for (i) type of the charmed particle produced in the given target; N_0 is the number of inelastic interactions in this target; $\sigma(i)$ is the cross-section for charmed particle (i) production at a single nucleon of the target; A is the atomic mass number of the AT material
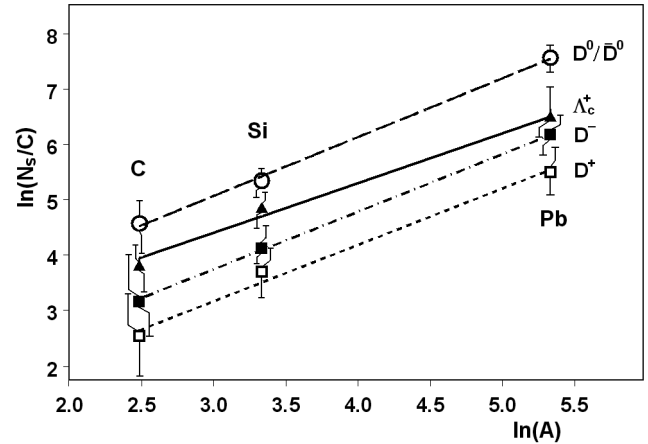

Fig. 7. The A-dependence of cross-sections for charmed particles production in pA-interactions.

Table 2. Characteristics of the charmed particles production. The first error is statistical, the second is the systematical one.

Type of charmed particle	Inclusive cross-section for all x_F (μb/nucleon)	α-parameter
D^+	$1.2 \pm 0.4 \pm 0.3$	$1.02 \pm 0.26 \pm 0.27$
D^-	$1.9 \pm 0.6 \pm 0.4$	$1.04 \pm 0.27 \pm 0.21$
D^0	$2.5 \pm 0.8 \pm 0.5$	$1.08 \pm 0.12 \pm 0.15$
$\bar{D}^0$	$4.6 \pm 1.6 \pm 0.9$	
Λ_c^+	$4.0 \pm 1.6 \pm 1.3$	$0.9 \pm 0.2 \pm 0.29$

Table 3. Summary of systematic uncertainties in charm production cross-sections.

Sources	$D^0 + \bar{D}^0$	D^+	D^-	Λ_c^+
Event fitting	12%	26%	19%	18%
Branching	1%	4%	4%	26%
Luminosity (K_tr)	6%	6%	6%	6%
Detection efficiency	3%	1%	2%	2%
TOTAL	14%	27%	20%	32%

(C, Si or Pb); $\alpha(i)$ is the exponent parameter in the A-dependence of the charm cross-section; $\sigma_{pp} = 31440\,\mu$b is the cross-section of inelastic proton-proton interactions at $70\,\mathrm{GeV}$ [17]; $B(i)$ is the branching ratio for the charmed particle decay ($B(D^0$ or $\bar{D}^0 \to K\pi) = 0.038$, $B(D^\pm \to K\pi\pi) = 0.094$, $B(\Lambda_c^+ \to pK^-\pi^+) = 0.05$); $\varepsilon(i)$ is the detection efficiency of the charmed particle from table 1 and $K_\mathrm{tr} = 0.57$ is the trigger efficiency for the selection of inelastic events.

Substituting $C(i) = [N_0/(\sigma_{pp} \times A^{0.7})] \times [(B(i) \times \varepsilon(i))/K_\mathrm{tr}]$, the relation takes the following form:

$$N_\mathrm{s}(i) = C(i) \times \sigma(i) \times A^\alpha, \quad \text{or}$$
$$\ln(N_\mathrm{s}(i)/C(i)) = \alpha \times \ln(A) + \ln(\sigma(i)).$$

Figure 7 shows the A-dependence of the charmed particles production in the AT.

The α-parameter, obtained from the straight linear approximations in fig. 7 for each particle, is presented in
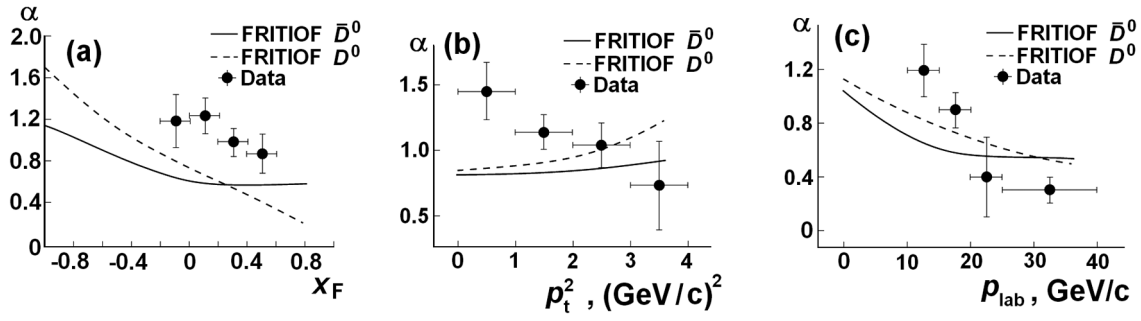
Fig. 8. The α-parameter as a function of (a) x_{F}, (b) p_{t}^2 and (c) p_{lab} for $(D^0 + \bar{D}^0)$ particles. The lines describe MC events (FRITIOF).

Table 4. The charmed particles yields, $\sigma(\mathrm{i})/\sigma_{\mathrm{tot}}(c\bar{c})$.

Particle yields	PYTHIA pp	FRITIOF pA	SVD-2 pA	Other experiments		
				NA-27 [18]	HERA-B [19]	
D^0	0.28	0.51	0.35 ± 0.16	0.57 ± 0.08	0.44 ± 0.18	
$\bar{D}^0$	0.74	0.59	0.65 ± 0.31	0.43 ± 0.09	0.54 ± 0.23	
D^+	0.13	0.29	0.16 ± 0.07	0.31 ± 0.06	0.19 ± 0.08	
D^-	0.24	0.27	0.27 ± 0.17	0.34 ± 0.06	0.25 ± 0.11	
Λ_c^+	0.55	0.36	0.56 ± 0.27	0.52 ± 0.35 BIS-2 [20,21]	0.42 ± 0.13 E-769 [22]	0.18 ± 0.01 SELEX-2 [23]

table 2 together with inclusive cross-sections, which are obtained as average value with three nucleus targets.

The total systematic uncertainties of the charm production cross-sections are composed of contributions from uncertainties in the signal yields (N_{s}) associated with the fitting procedure, from a systematic error of the number of inelastic events (N_0), from uncertainties in the branching ratio of decays and from uncertainties in the calculations of detection efficiencies. The individual contributions are summarized in table 3. The systematic error of N_{s} was estimated from the uncertainties of the number of background events under the signal peak with different fitting. The detection efficiency uncertainty was defined by modeling with PYTHIA and FRITIOF programs. The systematic uncertainties of the trigger factor (K_{tr}) give the uncertainties in N_0. They were estimated from multiplicity distributions for MC events and experimental data.

The α-parameters are consistent with 1 for all charmed particles, as was found earlier for hidden charm (J/ψ and ψ') production cross-sections in proton-nucleus interactions [24–27]. This supports the factorization theorem of perturbative QCD, which separates the perturbatively calculable short-distance quark and gluon interactions from non-perturbative dynamics.

For the largest number of the reconstructed mesons $(D^0 + \bar{D}^0)$ the dependence of the α-parameter on the kinematical variables (x_{F}, p_{t}^2 and P_{lab}) can be measured. According to [28] the x_{F}-dependence of α-parameters reflects the contributions to the cross-section from various sub-processes, such as final-state absorption, interactions with closely flying hadrons (comovers), shadowing of parton distributions, parton energy loss in the medium, and the effect of intrinsic charm components. Figure 8 shows

the x_{F}, p_{t}^2 and P_{lab} dependences of the α-parameter for D^0 or $\bar{D}^0$ particles in this experiment [29].

In fig. 8, the curves present the results of simulation with FRITIOF package. We observe that the α-parameter decreases with increasing x_{F} and p_{lab} over the entire range of measurements for these values. The simulations confirm this behavior qualitatively. For the p_{t}^2 dependence of the α-parameter there is no similarity between the model and the experimental data. There are only few measurements of the A-dependence on kinematical variables, summarized in [30]. The α-parameter behavior in these experiments differs from the present experiment, but one should note that these experiments were carried out at higher primary beam energies, in the range 250–600 GeV.

6 Total cross-section and ratios of charmed particles yields

The total cross-section of the charmed particles production [31] in proton-nucleon interactions at 70 GeV/c is determined as follows:

$$\sigma_{\mathrm{tot}}(c\bar{c}) = 1/2(\sigma_{D^+} + \sigma_{D^0} + \sigma_{D^-} + \sigma_{\bar{D}^0} + \sigma_{\Lambda_c^+} + \sigma_{D_s} + \sigma_{\bar{D}_s}).$$

By using the results presented in table 2, we obtain:

$$\sigma_{\mathrm{tot}}(c\bar{c}) = 7.1 \pm 2.3(\mathrm{stat}) \pm 1.5(\mathrm{syst}) \,\mu\mathrm{b/nucleon}.$$

The cross-section of the $D_s + \bar{D}_s$ meson production is not known for the relation above, but its contribution into $\sigma_{\mathrm{tot}}(c\bar{c})$ is not larger than 10% at this energy [31,19]. The charmed particle yields measured in our experiment are given in table 4 and in fig. 9 along with data from other experiments and theoretical predictions.
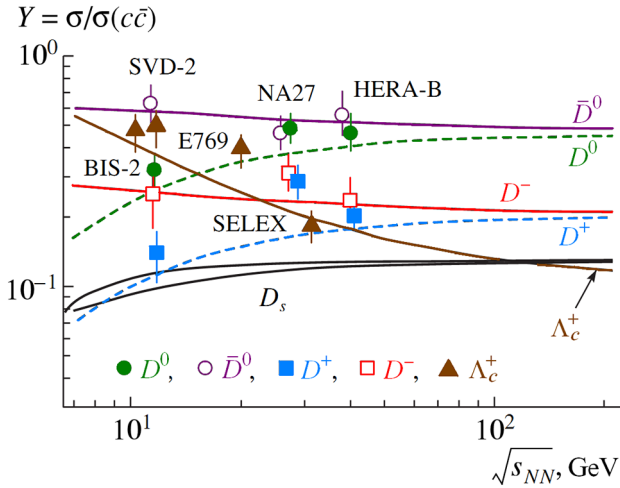
Fig. 9. Relative yields of charmed particles. The experimental points (●: D^0; ○: $\bar{D}^0$; ■: D^+; □: D^-; ▲: Λ_c^+) are taken from table 4, the theoretical curves (with designation of a particle) are taken from [32].

The contributions of charmed particles to the total cross-section display a dependence on energy. For example, the contributions of D^0 and D^+ mesons go down as the interaction energy decreases to $70\,\mathrm{GeV}$, while the contributions for their antiparticles, $\bar{D}^0$ and D^-, increase. A large difference of the charmed particle and antiparticle yields was firstly observed experimentally in neutron-nucleus interactions at the average neutron beam energy of $43\,\mathrm{GeV}$ in the BIS-2 experiment [33]. Only the antiparticle ($\bar{D}^0$ and D^-) decays were observed there, while particle (D^0 and D^+) decays were not found (their cross-sections proved to be below the sensitivity threshold). The nuclear matter effects on their production can explain this behavior of the charmed particles. The mechanisms of these effects were considered in [34–42]. The results shown in fig. 9 are compatible with the predictions of the statistical hadronization model [31,32].

The yield of Λ_c^+ baryons increases jointly with $\bar{D}^0$ and D^- meson contributions to the total cross-section with decreasing energy. This can indicate the growth of the $\Lambda_c^+ \bar{D}^0$ and $\Lambda_c^+ D^-$ pair production near the threshold energy. The cross-section of this pair production has been evaluated by means of the Quark-Gluon Strings Model (QGSM) [43,44]. The cross-section turns out to be larger than the prediction of QCD models by ten times. In this model the inclusive cross-section for Λ_c^+ at $\sqrt{s} \sim 10.0\,\mathrm{GeV}$ is $\sigma_\Lambda(\mathrm{incl}) \sim 10\,\mu\mathrm{b}$ and it is much closer to the experimental results of the SVD-2 and BIS-2 Collaborations.

The SVD-1 Collaboration, using the hydrogen rapid cycle bubble chamber, estimated the total cross-section for charm production in pp-interactions at $\sqrt{s} = 11.8\,\mathrm{GeV}$ as $1.6^{+1.1}_{-0.7}(\mathrm{stat}) \pm 0.3(\mathrm{syst})\,\mu\mathrm{b}$ [45]. This cross-section is compatible to QCD predictions. But all other estimations of the cross-section for open charm production at this energy (see fig. 10) are much above the QCD model predictions. The result of the SVD-1 Collaboration can be considered as lower limit only.
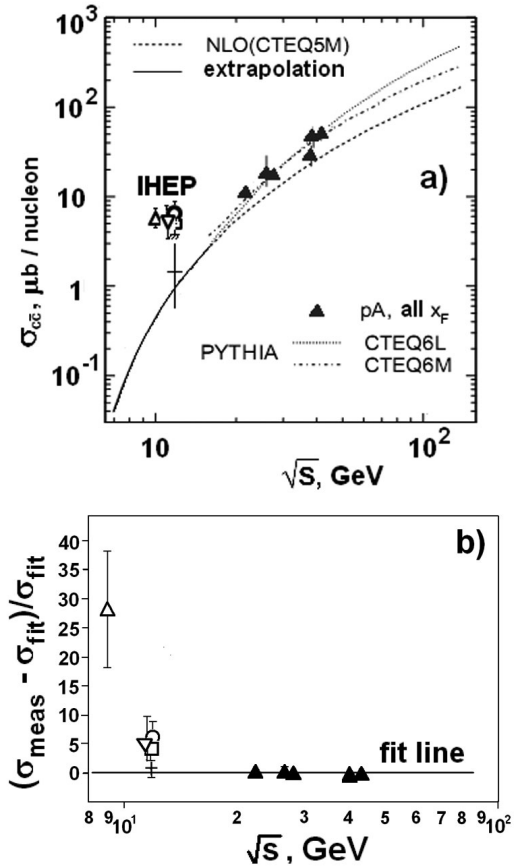

Fig. 10. (a) The total cross-section for the charm production in pA-interactions from [2–4,31]. Extrapolation (the solid line) was carried out in [31] without the points from IHEP: ○ — SVD-2 experiment (see above), ▽ —beam-dump experiment with a muon absorber [2], □ —SCAT bubble chamber experiment [3], △ —the experiment with BIS-2 spectrometer [4] and + —SVD-1 experiment [37]. Other lines are taken from various models [31]. (b) The normalized difference between the measured cross-sections and extrapolated curve from (a).

7 Summary

We have presented the total cross-section for the open charm production and cross-sections for the inclusive production of D mesons and Λ_c^+ baryons.

– As can be seen in fig. 10(a) and the data mentioned above: the total open charm production cross-section at the collision c.m. energy $\sqrt{s} \sim 10\,\mathrm{GeV}$ is above the QCD model predictions and the inclusive cross-sections are closer to the prediction of QGSM for D mesons and for Λ_c^+ baryon at this energy. The latest theoretical publication on this subject agrees with that conclusion [46]. To support this conclusion the normalized difference between the measured cross-sections and extrapolated curve from fig. 10(a) is shown in fig. 10(b). Despite of the large errors the difference becomes higher with decreasing collision energy.

– For $\sqrt{s} > 30\,\mathrm{GeV}$, there is an apparent discrepancy between the existing experimental measurements for
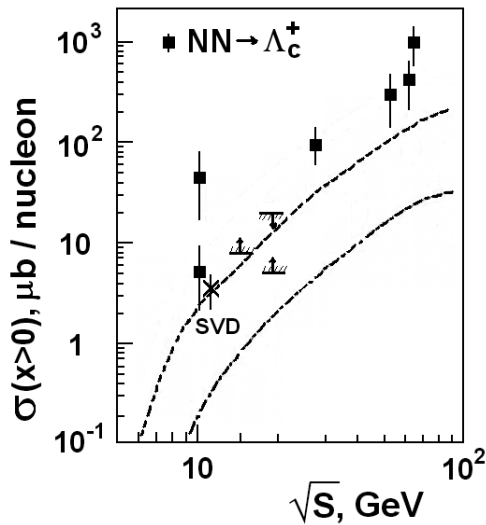
Fig. 11. The inclusive cross-section for Λ_c^+ baryon production at $x_F > 0$. The experimental data are taken from [20,21,47–53], point $\times$ is the result of our experiment. The dashed lines are predictions of two versions of the QCD model [20,21].

the Λ_c^+ cross-sections (fig. 11) and the measured total cross-sections for the open charm production reported in fig. 10(a).

– The observed behavior of the A-dependence of the α-parameter for the $D^0 + \bar{D}^0$ inclusive cross-section as a function of kinematical variables differs from that reported at higher energies [30].
– The relative yields of the charmed particles appear to be energy dependent.

References

1. J. Eschke, EPJ Web of Conferences **20**, 05002 (2012) arXiv:1607.01487 [nucl-ex].
2. A.E. Astratyan et al., Phys. Lett. B **79**, 497 (1978).
3. V.V. Ammosov et al., Phys. At. Nucl. **53**, 999 (1991).
4. A.N. Aleev et al., Phys. At. Nucl. **56**, 147 (1993).
5. C. Lourenco, H.K. Wohri, Phys. Rep. **433**, 127 (2006).
6. V.V. Avdeichikov et al., Instrum. Exp. Tech. **56**, 9 (2013).
7. H. Pi, Comput. Phys. Commun. **71**, 173 (1992).
8. OPAL Collaboration (G. Alexander et al.), Z. Phys. C **72**, 16 (1996).
9. G.S. Huang et al., Phys. Rev. Lett. **94**, 011802 (2005).
10. GEANT 3.21, CERN Program Library Long Write Up W5013.
11. A.A. Kiriakov et al., Instrum. Exp. Tech. **47**, 611 (2004).
12. A.P. Vorobiev et al., IHEP Preprint 2008-17, Protvino, 2008 (in Russian) http://web.ihep.su/library/pubs/prep2008/ps/2008-17.pdf.
13. V.N. Ryadovikov, Phys. At. Nucl. **73**, 1539 (2010) (on behalf of the SVD-2 Collaboration).
14. V.N. Ryadovikov, Phys. At. Nucl. **77**, 716 (2014) (on behalf of the SVD-2 Collaboration).
15. V.N. Ryadovikov, Phys. At. Nucl. **79**, 144 (2016) (on behalf of the SVD-2 Collaboration).
16. Particle Data Group (J. Beringer et al.), Phys. Rev. D **86**, 010001 (2012).
17. Yu.P. Gorin et al., Phys. At. Nucl. **14**, 998 (1971).
18. Na-27 Collaboration (M. Aguilar-Benitez), Phys. Lett. B **189**, 476 (1987).
19. I. Abt et al., Eur. Phys. J. C **52**, 531 (2007) arXiv:0708.1443v1.
20. BIS-2 Collaboration (A.N. Aleev et al.), Z. Phys. C **23**, 333 (1984).
21. N. Chudakov, Master's Thesis (1987), JINR Preprint 1-87-183, 1987 (in Russian).
22. J. Engelfried, www.ifisica.uaslp.mx/~jurgen/public/dpc99-talk.ps.gz (1999).
23. SELEX Collaboration (F.G. Garcia et al.), Phys. Lett. B **528**, 49 (2002). arXiv:hep-ex/0109017.
24. J. Badier et al., Z. Phys. C **20**, 101 (1983).
25. D.M. Alde et al., Phys. Rev. Lett. **66**, 133 (1991).
26. M.C. Abreu et al., Phys. Lett. B **410**, 327 (1997).
27. M.J. Leitch et al., Nucl. Phys. A **544**, 197 (1992).
28. R. Vogt, Phys. Rev. C **61**, 035203 (2000).
29. SVD-2 Collaboration (A.N. Aleev et al.), Phys. At. Nucl. **74**, 324 (2011).
30. SELEX Collaboration (A. Blanco-Covarrubias et al.), Eur. Phys. J. C **64**, 637 (2009) arXiv:0902.0355v1.
31. A. Andronic, P. Braun-Munzinger, K. Redlich, J. Stachel, Phys. Lett. B **659**, 149 (2008) arXiv:0708.1488.
32. A. Andronic, F. Beutler, P. Braun-Munzinger et al., arXiv:0904.1368v2.
33. A. Aleev et al., Z. Phys. C **37**, 243 (1988).
34. L. Tolos, J. Schaffner-Bielich, H. Stocker, Phys. Lett. B **635**, 85 (2006) arXiv:nucl-th/0509054.
35. K. Tsushima, D.H. Lu, A.W. Thomas et al., Phys. Rev. C **59**, 2824 (1999) arXiv:nucl-th/9810016.
36. A. Sibirtsev, K. Tsushima, A.W. Thomas, Eur. Phys. J. A **6**, 351 (1999) arXiv:nucl-th/9904016.
37. A. Sibirtsev, K. Tsushima, K. Saito, A.W. Thomas, Phys. Lett. B **484**, 23 (2000) arXiv:nucl-th/9904015.
38. A. Hayashigaki, Phys. Lett. B **487**, 96 (2000) arXiv:nucl-th/0001051.
39. W. Cassing, E.L. Bratkovskaya, A. Sibirtsev, Nucl. Phys. A **691**, 753 (2001) arXiv:nucl-th/0010071.
40. B. Friman, S.H. Lee, T. Song, Phys. Lett. B **548**, 153 (2002) arXiv:nucl-th/0207006.
41. M.F.M. Lutz, C.L. Korpa, Phys. Lett. B **633**, 43 (2006) arXiv:nucl-th/0510006.
42. K. Morita, S.H. Lee, arXiv:0704.2021.
43. A.B. Kaidalov, O.I. Piskunova, Yad. Fiz. **43**, 1545 (1986) (in Russian).
44. A.M. Gasparyan et al., Eur. Phys. J. A **18**, 305 (2003) arXiv:nucl-th/0210018v1.
45. N.S. Amaglobeli et al., Phys. At. Nucl. **64**, 891 (2001).
46. Mohammed Younus et al., J. Phys. G: Part. Nucl. Phys. **39**, 025001 (2012) arXiv:1108.0855v2.
47. Bailay R. et al., Nucl. Phys. B **239**, 15 (1984).
48. E769 Collaboration (G.A. Alves et al.), Phys. Rev. Lett. **77**, 2388 (1996) 2392 (1996).
49. T. Aziz et al., Nucl. Phys. B **199**, 424 (1982).
50. M. Basile et al., Lett. Nuovo Cimento **30**, 487 (1981).
51. M. Basile et al., Lett. Nuovo Cimento **30**, 481 (1981).
52. F. Muller, Proceedings of IV Warsaw Symposium, 24–31 May 1981, Kazimierz, Poland (Institute of Theoretical Physics, Warsaw University, 1981).
53. G. Bari et al., Nuovo Cimento A **104**, 571 (1991).